

Article

Solution of Two-Dimensional Solute Transport Model for Heterogeneous Porous Medium Using Fractional Reduced Differential Transform Method

Manan A. Maisuria ¹, Priti V. Tandel ^{1,*} and Trushitkumar Patel ²

¹ Department of Mathematics, Veer Narmad South Gujarat University, Surat 395007, India; mananmaisuria.maths21@vnsgu.ac.in

² Department of General Studies, University of the People, Pasadena, CA 91101, USA; trushitkumar.patel@uopeople.edu

* Correspondence: pvtandel@vnsgu.ac.in

Abstract: This study contains a two-dimensional mathematical model of solute transport in a river with temporally and spatially dependent flow, explicitly focusing on pulse-type input point sources with a fractional approach. This model is analyzed by assuming an initial concentration function as a declining exponential function in both the longitudinal and transverse directions. The governing equation is a time-fractional two-dimensional advection–dispersion equation with a variable form of dispersion coefficients, velocities, decay constant of the first order, production rate coefficient for the solute at the zero-order level, and retardation factor. The solution of the present problem is obtained by the fractional reduced differential transform method (FRDTM). The analysis of the initial retardation factor has been carried out via plots. Also, the influence of initial longitudinal and transverse dispersion coefficients and velocities has been examined by graphical analysis. The impact of fractional parameters on pollution levels is also analyzed numerically and graphically. The study of convergence for the FRDTM technique has been conducted to assess its efficacy and accuracy.

Keywords: advection; dispersion; heterogeneous medium; fractional reduced differential transform method (FRDTM)

MSC: 35A22; 35C10; 35R11



Citation: Maisuria, M.A.; Tandel, P.V.; Patel, T. Solution of Two-Dimensional Solute Transport Model for Heterogeneous Porous Medium Using Fractional Reduced Differential Transform Method. *Axioms* **2023**, *12*, 1039. <https://doi.org/10.3390/axioms12111039>

Academic Editor: Rafael Granero-Belinchón

Received: 10 October 2023
Revised: 30 October 2023
Accepted: 5 November 2023
Published: 8 November 2023



Copyright: © 2023 by the authors. Licensee MDPI, Basel, Switzerland. This article is an open access article distributed under the terms and conditions of the Creative Commons Attribution (CC BY) license (<https://creativecommons.org/licenses/by/4.0/>).

1. Introduction

Several authors have examined a space–time fractional partial differential equation. The fundamental partial differential equation may be changed by replacing the second-order space-derivative and first-order time-derivative with fractional derivatives of order $\beta > 0$ and $\alpha > 0$, respectively [1]. Authors have obtained a numerical solution of the one-dimensional fractional advection–dispersion equations with variable coefficients on a finite domain [2]. Fractional space derivatives represent anomalous diffusion or dispersion models, in which a particle plume spreads at a rate inconsistent with the classical Brownian motion model. In groundwater hydrology, fractional advection–dispersion equations represent passive tracer transfer in porous fluid flow. For a one-dimensional advection–dispersion model with constant coefficients, Fourier transform techniques provide analytical solutions [3,4].

Research on the transport of contaminants through porous media using hydraulic permeability is very significant for many technical, biophysical, and biological purposes. These include the treatment of contaminants, extraction of oil, and the management of high-level nuclear waste disposal [5]. Solute transport in disordered porous media is crucial in many scientific and engineering fields. Some of its examples are Tracer investigations in oil recovery, subsurface pollutant transfer, chemical transport in packed bed reactors, water filtering, fuel cells, and current catalyst development [6].

Several mathematical models have been created to study contaminant transport in porous media during groundwater flow, focusing on pollutant migration mechanisms. Djordjević and Savović have derived numerical solutions for the one-dimensional advection–diffusion equation with variable coefficients in semi-infinite media. The equation includes the dependence of flow on both time and space. The authors have used the explicit finite difference method to obtain the solution [7]. A numerical solution for two-dimensional solute transport was developed using finite difference techniques with periodic velocity in homogeneous porous media [8]. Two-dimensional solute transport was modeled mathematically in semi-infinite heterogeneous porous media. It has geographically and time-dependent coefficients for various input concentration pulses [9]. The Galerkin spectral element approach is used to provide an approximation of the Riesz space fractional in spatial directions, primarily to calculate the fractional advection–dispersion equation that applies in one and two dimensions of Riesz space [10]. For the alternative way to analyze the two-dimensional time distributed-order diffusion-wave equation, authors have also applied the Legendre–Laguerre spectral method over a semi-infinite domain [11]. The analysis of memory-based two-dimensional advection–diffusion equations inside a domain with a source located at the symmetry center of the domain is carried out by using Laplace and double sine-Fourier transformations [12].

There are multiple advantages to studying two-dimensional contaminant transport models over one-dimensional models. Two-dimensional models involve concentration gradients and contaminant transport in the orthogonal direction of the groundwater flow. Many researchers have analyzed two-dimensional models with longitudinal velocity components, neglecting the transverse velocity components. In the present problem, we have considered the dispersion coefficients as a linear multiple of spatially dependent function and seepage velocity and velocity components as the n th power of spatially dependent function. This is analyzed using the FRDTM, an advanced and effective method to identify solutions for the time-fractional two-dimensional advection–diffusion equation. Our research’s primary contribution is forecasting water behavior, which has significant implications for preserving water quality in environmental systems. We have also analyzed the effect of various factors on river pollution reduction.

In the context of modeling, fluid flow, and solute transport in porous media, the time-fractional part allows for the inclusion of subdiffusion phenomena. Subdiffusion refers to the phenomenon where the movement of fluid and solute particles is hindered, resulting in slower rates of advection and diffusion compared to classical scenarios. This hindrance may be attributed to many factors, such as obstacles or heterogeneities within the medium.

Fractional-order models provide greater flexibility in capturing complex dynamic behaviors due to their continuous nature, which can be more representative of real-world dynamics. Nonlinear fractional partial differential equations are often more challenging than linear ones. Moreover, no method gives an exact solution for the fractional-order differential equation. Hence, nonlinear PDEs of fractional order make the research more significant. They can describe systems with memory and hereditary properties more accurately. Fractional-order models explicitly capture non-local memory effects, while integer-order models assume local memory. However, there are some drawbacks to fractional-order models. They can be more mathematically complex and challenging to analyze compared to integer-order models. It requires specialized techniques to solve fractional-order differential equations.

In this paper, we have applied the latest technique, namely the FRDTM—an efficient and robust method to find the solutions of the time-fractional two-dimensional advection–dispersion equation. The FRDTM provides highly accurate numerical results for nonlinear time-fractional differential equations without spatial discretization, linearization, transformation, or perturbation. The FRDTM can be applied to derive a variety of fractional-order nonlinear problems with distinct physical structures arising in science, which is the novelty of our work.

The remainder of this paper is structured as follows: Section 2 discusses the mathematical construction of the model. Section 3 revisits several fundamental concepts and

features of the FRDTM. Section 4 discusses the numerical results and their consequences. Section 5 closes with concluding comments.

2. Mathematical Construction of the Problem

The two primary mechanisms by which contaminants penetrate the subsurface are advection, which is brought on by groundwater movement, and dispersion, which results from mechanical mixing and molecular diffusion, both occurring simultaneously. The small seepage velocity precludes the investigation of molecular diffusions. The two-dimensional advection–diffusion equation can have its mathematical form provided by a parabolic partial differential equation of the second order. It is expressed as [13]

$$R^* \frac{\partial c}{\partial \tau} = \frac{\partial}{\partial x} \left(D_x^* \frac{\partial c}{\partial x} - u^* c \right) + \frac{\partial}{\partial y} \left(D_y^* \frac{\partial c}{\partial y} - v^* c \right) - \alpha^* c + \beta^* \tag{1}$$

The variable c (mg L^{-1}) represents the solute concentration of the pollutant as it is transported through the medium along the flow field at any given place (x, y) and time τ . D_x^* ($\text{m}^2 \text{ day}^{-1}$) and D_y^* ($\text{m}^2 \text{ day}^{-1}$) represent the longitudinal and transverse dispersion coefficients, respectively. Additionally, the parameters u^* (m day^{-1}) and v^* (m day^{-1}) values represent the unstable uniform seepage velocity in the longitudinal and transverse directions, respectively. The value α^* (day^{-1}) represents the decay constant of the first order, while the parameter β^* ($\text{kg m}^{-3} \text{ day}^{-1}$) identifies the production rate coefficient for the solute at the zero-order level which represents the production of the solute internally or externally in the medium. The dimensionless quantity known as the retardation factor is symbolized by R^* .

Consider the spatial and temporal dependencies of the flow domain parameters as under [13]

$$\begin{aligned} D_x^* &= D_{x_0}(1+ax)^3(1+by)g(m\tau), D_y^* = D_{y_0}(1+by)^3(1+ax)g(m\tau), \\ u^* &= u_0(1+ax)^2(1+by)g(m\tau), v^* = v_0(1+by)^2(1+ax)g(m\tau), \\ R^* &= R_0(1+ax)(1+by), \alpha^* = \alpha_0(1+ax)(1+by)g(m\tau), \beta^* = \beta_0(1+ax)(1+by)g(m\tau) \end{aligned} \tag{2}$$

The parameters a and b represent heterogeneity in the longitudinal and transverse directions. The varied values of a and b reflect various levels of heterogeneity. The heterogeneity of the porous media refers to the condition where the porosity or hydraulic conductivity varies based on the specific location within the medium. Initial dispersion coefficients in the longitudinal and transverse directions are denoted by the symbols D_{x_0} and D_{y_0} , respectively. Initial unstable uniform seepage velocities in the longitudinal and lateral directions are denoted by the notation u_0 and v_0 , respectively. The parameter for unsteadiness is denoted by m . The initial decay constant of the first order and the zero-order production rate coefficient for the solute are denoted by the notations α_0 and β_0 , respectively. R_0 is the initial retardation factor. We assumed $g(m\tau)$, where $g(m\tau) = 1$ when $\tau = 0$ or $m = 0$. The first situation depicts a steady flow, while the second represents the initial state. $g(m\tau)$ is an expression without dimensions. Therefore, Equation (1) is converted into the given form.

$$\begin{aligned} \frac{R_0}{g(m\tau)} \frac{\partial c}{\partial \tau} &= D_{x_0}(1+ax)^2 \frac{\partial^2 c}{\partial x^2} + D_{y_0}(1+by)^2 \frac{\partial^2 c}{\partial y^2} + (3D_{x_0}a - u_0)(1+ax) \frac{\partial c}{\partial x} \\ &+ (3D_{y_0}b - v_0)(1+by) \frac{\partial c}{\partial y} - 2(au_0 + bv_0)c - \alpha_0 c + \beta_0 \end{aligned} \tag{3}$$

Let us introduce new variables defined as under [13].

$$X = \frac{\log(1+ax)}{a}, Y = \frac{\log(1+by)}{b} \text{ and } T = \int_0^\tau g(m\tau) d\tau.$$

Hence, Equation (3) transforms into the given form using the provided transformations.

$$R_0 \frac{\partial c}{\partial T} = D_{x_0} \frac{\partial^2 c}{\partial X^2} + D_{y_0} \frac{\partial^2 c}{\partial Y^2} - (u_0 - 2aD_{x_0}) \frac{\partial c}{\partial X} - (v_0 - 2bD_{y_0}) \frac{\partial c}{\partial Y} - 2(au_0 + bv_0)c - \alpha_0 c + \beta_0 \tag{4}$$

The initial values of the function $c(X, Y, T)$ are supposed to follow a declining exponential pattern with respect to both X and Y [14].

$$c(X, Y, 0) = e^{-\frac{(X+Y)}{\gamma_0}} \tag{5}$$

3. Fractional Reduced Differential Transform Method (FRDTM)

Some of the basic ideas and characteristics of the theory of fractional calculus are explained in this section [15,16].

Definition 1. The fractional derivative of the function w of order λ , in the sense of Caputo, is denoted by $D^\lambda w(\tau)$ and is defined as

$$D^\lambda w(\tau) = \frac{1}{\Gamma(n - \lambda)} \int_0^1 (\tau - t)^{n-1} w^n(t) dt, \tag{6}$$

for $n - 1 < \lambda \leq n, n \in \mathbb{N}$

Let us consider a function of three variables, denoted as $\omega(\vartheta, \omega, \tau)$, which can be expressed as the product of three single-variable functions, i.e., $\omega(\vartheta, \omega, \tau) = s(\vartheta)k(\omega)u(\tau)$. The representation of function $\omega(\vartheta, \omega, \tau)$ may be determined based on the characteristics of differential transform.

$$\omega(\vartheta, \omega, \tau) = \sum_{n=0}^{\infty} \Omega_n(\vartheta, \omega) \tau^{\lambda n} \tag{7}$$

where $\Omega_n(\vartheta, \omega)$ is a t -dimensional spectrum function. $\Omega_n(\vartheta, \omega)$ is the transformed function of $\omega(\vartheta, \omega, \tau)$. The basic definitions and operations of the FRDTM are as follows:

The R_D operator signifies the reduced differential transform, whereas the R_D^{-1} denotes the inverse reduced differential transform.

Definition 2. Let us examine the function $\omega(\vartheta, \omega, \tau)$, which is assumed to possess analyticity and continuous differentiability with respect to ϑ, ω , and τ inside the selected domain. The definition of the reduced differential transformations for the function $\omega(\vartheta, \omega, \tau)$ is as follows [17,18]:

$$R_D[\omega(\vartheta, \omega, \tau)] \approx \Omega_n(\vartheta, \omega) = \frac{1}{\Gamma(\lambda n + 1)} \left[\frac{\partial^{\lambda n}}{\partial \tau^{\lambda n}} \omega(\vartheta, \omega, \tau) \right]_{\tau=0} \tag{8}$$

The symbol λ is used to denote the time-fractional-order derivative.

Definition 3. The following is a presentation of the inverse differential transformations of the function $\Omega_n(\vartheta, \omega)$:

$$R_D^{-1}[\Omega_n(\vartheta, \omega)] \approx \omega(\vartheta, \omega, \tau) = \sum_{n=0}^{\infty} \Omega_n(\vartheta, \omega) \tau^{\lambda n} \tag{9}$$

From Equations (8) and (9), we obtain

$$\omega(\vartheta, \omega, \tau) = \sum_{n=0}^{\infty} \frac{1}{\Gamma(\lambda n + 1)} \left[\frac{\partial^{\lambda n}}{\partial \tau^{\lambda n}} \omega(\vartheta, \omega, \tau) \right]_{\tau=0} \tau^{\lambda n} \tag{10}$$

In order to elucidate the fundamental principles of the FRDTM, let us examine the following nonlinear partial differential equation expressed in an operator format [19]:

$$L\omega(\vartheta, \omega, \tau) + H\omega(\vartheta, \omega, \tau) + W\omega(\vartheta, \omega, \tau) = f(\vartheta, \omega, \tau) \tag{11}$$

with initial condition $\omega(\vartheta, \omega, 0) = h(\vartheta, \omega)$ (12)

where $L = \frac{\partial^\lambda}{\partial \tau^\lambda}$, the linear operator H has partial derivatives, whereas the operator $W\omega(\vartheta, \omega, \tau)$ is nonlinear, and $f(\vartheta, \omega, \tau)$ represents an inhomogeneous term.

Based on the principles of the FRDTM, it is possible to derive the following iteration formula:

$$\frac{\Gamma(\lambda(n + 1) + 1)}{\Gamma(\lambda n + 1)} \Omega_{n+1}(\vartheta, \omega) = F_n(\vartheta, \omega) - H\Omega_n(\vartheta, \omega) - W\Omega_n(\vartheta, \omega) \tag{13}$$

The functions $\Omega_n(\vartheta, \omega)$, $H\Omega_n(\vartheta, \omega)$, $W\Omega_n(\vartheta, \omega)$, and $F_n(\vartheta, \omega)$ represent the transformations of the functions $\omega(\vartheta, \omega, \tau)$, $H\omega(\vartheta, \omega, \tau)$, $W\omega(\vartheta, \omega, \tau)$, and $f(\vartheta, \omega, \tau)$, respectively. Based on the initial condition (12), we formulate

$$\Omega_0(\vartheta, \omega) = h(\vartheta, \omega) \tag{14}$$

By substituting Equation (14) into Equation (13) and conducting a basic iterative computation, we get the values of $\Omega_n(\vartheta, \omega)$ as follows. Subsequently, the inverse translation of the set of values $\{\Omega_n(\vartheta, \omega)\}_{n=0}^k$ yields the k -terms approximation solution in the following manner:

$$\omega_k(\vartheta, \omega, \tau) = \sum_{n=0}^k \Omega_n(\vartheta, \omega) \tau^{\lambda n} \tag{15}$$

Hence, the exact answer is given by

$$\omega(\vartheta, \omega, \tau) = \lim_{k \rightarrow \infty} \omega_k(\vartheta, \omega, \tau) \tag{16}$$

Theorem 1. If $\omega(\vartheta, \omega, \tau) = \sum_{n=0}^{\infty} \Omega_n(\vartheta, \omega) \tau^{\lambda n}$ is given series [20–22]:

1. Given series solution is convergent if $\exists 0 < \alpha < 1$ such that $\frac{\|\Omega_{n+1}\|}{\|\Omega_n\|} \leq \alpha$.
2. Given series solution is divergent if $\exists \alpha > 1$ such that $\frac{\|\Omega_{n+1}\|}{\|\Omega_n\|} \geq \alpha$.

The proof of Theorem 1, which is a particular case of Banach’s fixed point theorem, can be found in the reference.

Corollary 1. The series solution $\sum_{n=0}^{\infty} \Omega_n(\vartheta, \omega, \tau)$ exhibits convergence toward the exact solution $\omega(\vartheta, \omega, \tau)$ with the condition that $0 \leq \zeta_k < 1$, where every k belongs to the whole number [20–22].

$$\zeta_k = \begin{cases} \frac{\|\Omega_{k+1}\|}{\|\Omega_k\|}, & \|\Omega_k\| \neq 0 \\ 0, & \|\Omega_k\| = 0 \end{cases}$$

Table 1 presents the essential mathematical operations of the FRDTM, providing simple accessibility.

Table 1. Transform table [23–26].

Function	Transformation
$\omega(\vartheta, \omega, \tau)$	$\Omega_j(\vartheta, \omega) = \frac{1}{\Gamma(\lambda j + 1)} \left[\frac{\partial^{j\lambda}}{\partial \tau^{j\lambda}} \omega(\vartheta, \omega, \tau) \right]_{\tau=0}$
$\alpha\phi \pm \beta\zeta$	$\alpha\Phi_j \pm \beta\Xi_j$, α and β are constant.
$\phi(\vartheta, \omega, \tau)\zeta(\vartheta, \omega, \tau)$	$\sum_{n=0}^j \Phi_n(\vartheta, \omega)\Xi_{j-n}(\vartheta, \omega)$
$\frac{\partial^{\lambda n}}{\partial \tau^{\lambda n}} \omega(\vartheta, \omega, \tau)$	$\frac{\Gamma(j\lambda + n\lambda + 1)}{\Gamma(j\lambda + 1)} \Omega_{j+n}(\vartheta, \omega)$
$\frac{\partial^n}{\partial \vartheta^n} \omega(\vartheta, \omega, \tau)$	$\frac{\partial^n}{\partial \vartheta^n} \Omega_j(\vartheta, \omega)$.
$\frac{\partial^n}{\partial \omega^n} \omega(\vartheta, \omega, \tau)$	$\frac{\partial^n}{\partial \omega^n} \Omega_j(\vartheta, \omega)$.
$\vartheta^m \omega^p \tau^n$	$\vartheta^m \omega^p \delta(j\lambda - n)$ where $\delta(j\lambda - n) = \begin{cases} 1 & j\lambda = n \\ 0, & j\lambda \neq n \end{cases}$.

4. Results and Discussion

This part illustrates the numerical and graphical outcomes of the derived general solution, which includes several parameters. The impact of various parameters on the concentration profile has also been observed. In order to analyze this, Equation (4) was transformed into time-fractional partial differential equations, which are presented as follows:

$$R_0 \frac{\partial^\lambda c}{\partial T^\lambda} = D_{x_0} \frac{\partial^2 c}{\partial X^2} + D_{y_0} \frac{\partial^2 c}{\partial Y^2} - (u_0 - 2aD_{x_0}) \frac{\partial c}{\partial X} - (v_0 - 2bD_{y_0}) \frac{\partial c}{\partial Y} - 2(au_0 + bv_0)c - \alpha_0 c + \beta_0 \tag{17}$$

Applying the FRDTM on both sides of Equation (17), we obtain

$$R_0 \frac{\Gamma(\lambda(n+1)+1)}{\Gamma(\lambda n+1)} C_{n+1} = D_{x_0} \frac{\partial^2 C_n}{\partial X^2} + D_{y_0} \frac{\partial^2 C_n}{\partial Y^2} - (u_0 - 2aD_{x_0}) \frac{\partial C_n}{\partial X} - (v_0 - 2bD_{y_0}) \frac{\partial C_n}{\partial Y} - 2(au_0 + bv_0)C_n - \alpha_0 C_n + \beta_0 \delta(n\lambda) \tag{18}$$

$$C_{n+1} = \frac{\Gamma(\lambda n+1)}{R_0 \Gamma(\lambda(n+1)+1)} [D_{x_0} \frac{\partial^2 C_n}{\partial X^2} + D_{y_0} \frac{\partial^2 C_n}{\partial Y^2} - (u_0 - 2aD_{x_0}) \frac{\partial C_n}{\partial X} - (v_0 - 2bD_{y_0}) \frac{\partial C_n}{\partial Y} - 2(au_0 + bv_0)C_n - \alpha_0 C_n + \beta_0 \delta(n\lambda)] \tag{19}$$

From the initial condition (5), we obtain

$$C_0 = e^{-\frac{(X+Y)}{\gamma_0}} \tag{20}$$

From Equation (19) and (20), we obtain the general solution

$$c(X, Y, T) = C_0(X, Y) + C_1(X, Y)T^\lambda + C_2(X, Y)T^{2\lambda} + \dots = \Phi_0 + \Phi_1 + \Phi_2 + \dots \tag{21}$$

where

$$C_0 = e^{-\frac{(X+Y)}{\gamma_0}}$$

$$C_1 = \frac{e^{-\frac{X+Y}{\gamma_0}} \left(D_{x_0} + D_{y_0} + \gamma_0 u_0 + \gamma_0 v_0 - \alpha_0 \gamma_0^2 + \gamma_0^2 \beta_0 e^{\frac{X+Y}{\gamma_0}} - 2aD_{x_0} \gamma_0 - 2bD_{y_0} \gamma_0 - 2a\gamma_0^2 u_0 - 2b\gamma_0^2 v_0 \right)}{\gamma_0^2 R_0 \Gamma(\lambda+1)}$$

$$C_2 = \frac{e^{-\frac{X+Y}{\gamma_0}} (\alpha_0 + 2a u_0 + 2b v_0) \left(\alpha_0 + 2a u_0 + 2b v_0 - \beta_0 e^{\frac{X+Y}{\gamma_0}} \right)}{R_0^2 \Gamma(2\lambda+1)} + \frac{e^{-\frac{X+Y}{\gamma_0}} (D_{x_0} + D_{y_0})^2}{\gamma_0^4 R_0^2 \Gamma(2\lambda+1)}$$

$$- \frac{e^{-\frac{X+Y}{\gamma_0}} \left(4a^2 D_{x_0}^2 - 8abD_{x_0}D_{y_0} + 8aD_{x_0}u_0 + 4aD_{x_0}v_0 + 4aD_{y_0}u_0 - 4b^2 D_{y_0}^2 + 4bD_{x_0}v_0 + 4bD_{y_0}u_0 + 8bD_{y_0}v_0 + 2\alpha_0 D_{x_0} + 2\alpha_0 D_{y_0} - u_0^2 - 2u_0v_0 - v_0^2 \right)}{\gamma_0^2 R_0^2 \Gamma(2\lambda+1)}$$

$$+ \frac{2e^{-\frac{X+Y}{\gamma_0}} (D_{x_0} + D_{y_0}) (u_0 + v_0 - 2aD_{x_0} - 2bD_{y_0})}{\gamma_0^3 R_0^2 \Gamma(2\lambda+1)} - \frac{2e^{-\frac{X+Y}{\gamma_0}} (\alpha_0 + 2a u_0 + 2b v_0) (u_0 + v_0 - 2aD_{x_0} - 2bD_{y_0})}{\gamma_0 R_0^2 \Gamma(2\lambda+1)}$$

Furthermore, in order to perform a convergence analysis of a given series solution, we calculate the terms ζ_k using corollary 1. $\zeta_0 = \frac{\|\Phi_1\|}{\|\Phi_0\|} = 0.2057 < 1$, $\zeta_1 = \frac{\|\Phi_2\|}{\|\Phi_1\|} = 0.2054 < 1$. This observation confirms that the FRDTM yields a series solution that exhibits convergence toward the exact solution. Now, we have obtained the numerical values of the concentration for fixed $R_0 = 1.15, u_0 = 1.05, v_0 = 0.105, \alpha_0 = 0.01, D_{x_0} = 1.25, D_{y_0} = 0.125, \gamma_0 = 1.02, a = b = 0.01$ and $\beta_0 = 0.0021$ [13].

Tables 2–4 give the numerical values of concentration at fixed $(Y = 0.33, T = 0.2)$, $(Y = 0.55, T = 0.4)$, and $(Y = 0.77, T = 0.3)$ for different values of λ , respectively. We have shown a negative correlation between the change in X and the change in concentration. As Y continues to rise, the concentration will continue to fall. If there is an increase in T ,

there is also an increase in concentration. Additionally, we saw that the concentration was becoming lower as the λ value increased.

Table 2. $c(X, 0.33, 0.2)$.

X	$\lambda = 0.11$	$\lambda = 0.33$	$\lambda = 0.66$	$\lambda = 0.88$	$\lambda = 1$
0.1	3.980477607	2.607343465	1.454181455	1.099631673	0.98151519
0.2	3.60889774	2.363961035	1.318444752	0.996983733	0.88988869
0.3	3.272018472	2.143307276	1.195384045	0.903921741	0.80681889
0.4	2.96659923	1.943259632	1.083815565	0.819550497	0.7315067
0.5	2.689702069	1.761893767	0.982666092	0.7430584	0.66322765
0.6	2.438663406	1.597465053	0.89096263	0.673709644	0.60132496
0.7	2.211068402	1.448391786	0.807823046	0.610837137	0.54520316
0.8	2.004727734	1.313239971	0.73244759	0.553836082	0.49432238
0.9	1.817656529	1.190709532	0.664111196	0.502158164	0.44819319
1	1.648055278	1.079621801	0.602156508	0.455306275	0.40637185

Table 3. $c(X, 0.55, 0.4)$.

X	$\lambda = 0.11$	$\lambda = 0.33$	$\lambda = 0.66$	$\lambda = 0.88$	$\lambda = 1$
0.1	3.567649774	2.782692086	1.752639746	1.312338402	1.1429389
0.2	3.234633278	2.5229612	1.589067531	1.189862087	1.03627113
0.3	2.932716077	2.287485712	1.440770778	1.078823425	0.93956471
0.4	2.658993912	2.07400049	1.306322961	0.978154291	0.85188937
0.5	2.410833743	1.880451938	1.184430776	0.886886311	0.77240174
0.6	2.185848421	1.704978238	1.073921694	0.804141542	0.70033719
0.7	1.981873725	1.545891438	0.973732685	0.729124029	0.63500251
0.8	1.796947542	1.401661222	0.882899991	0.661112151	0.57576922
0.9	1.629290996	1.270900182	0.800549859	0.599451675	0.52206752
1	1.477291334	1.152350478	0.72589013	0.543549463	0.47338085

Table 4. $c(X, 0.77, 0.3)$.

X	$\lambda = 0.11$	$\lambda = 0.33$	$\lambda = 0.66$	$\lambda = 0.88$	$\lambda = 1$
0.1	2.750852231	1.988701837	1.177128614	0.878166651	0.77053285
0.2	2.494109165	1.803107244	1.067284338	0.796218808	0.6986261
0.3	2.261342475	1.634844708	0.967698051	0.7219238	0.63343449
0.4	2.050313086	1.482295647	0.877411794	0.654566954	0.5743309
0.5	1.858991025	1.343992632	0.795557068	0.593500337	0.5207468
0.6	1.685535891	1.218605273	0.721346481	0.538136528	0.47216674
0.7	1.52827915	1.104927418	0.654066172	0.487942959	0.42812341
0.8	1.38570809	1.001865558	0.593068946	0.4424368	0.38819314
0.9	1.256451263	0.9084283	0.537768046	0.401180308	0.35199182
1	1.139265299	0.823716834	0.487631512	0.363776622	0.31917122

Figure 1 presents a three-dimensional depiction of the concentration profile at various time points (T). Figures 2 and 3 provide visual depictions of concentration variations

for distinct values of X and Y , respectively. The value of variable c exhibits a positive correlation with the value of variable T , wherein a rise in T results in a corresponding increase in the value of c . The value of variable c exhibits a negative correlation with the values of variables X and Y as the latter two variables grow.

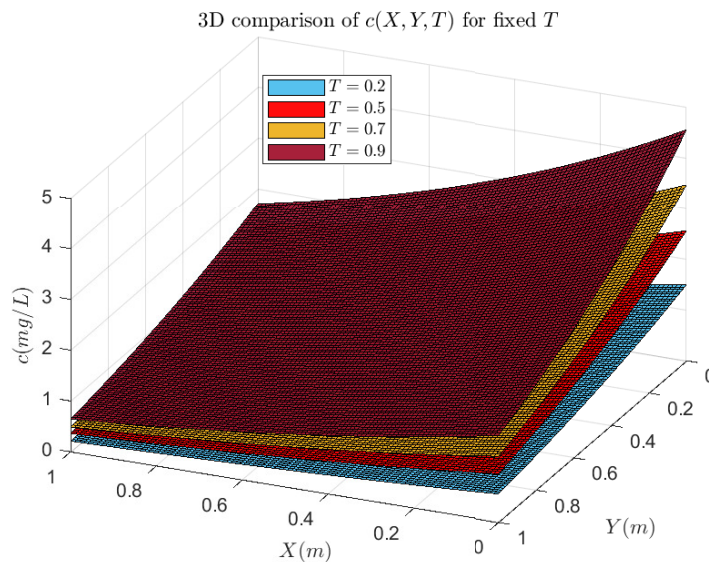


Figure 1. Three-dimensional comparison of approximate solution for different values of $T = 0.2, 0.5, 0.7,$ and 0.9 for $R_0 = 1.15, u_0 = 1.05, v_0 = 0.105, \alpha_0 = 0.04, D_{x_0} = 1.25, D_{y_0} = 0.125, a = b = 0.01, \lambda = 1, \gamma_0 = 1.02,$ and $\beta_0 = 0.0021$.

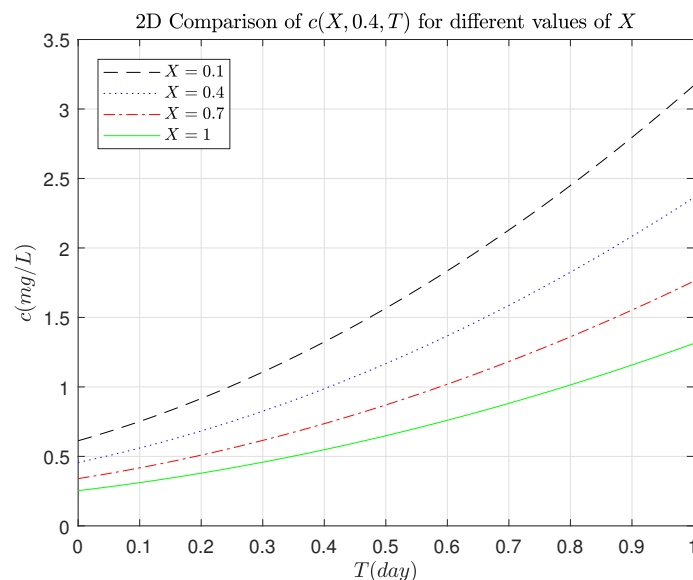


Figure 2. Two-dimensional comparison of approximate solution for different values of $X = 0.1, 0.4, 0.7,$ and 1 for $R_0 = 1.15, u_0 = 1.05, v_0 = 0.105, \alpha_0 = 0.04, D_{x_0} = 1.25, D_{y_0} = 0.125, a = b = 0.01, \lambda = 1, \gamma_0 = 1.02,$ and $\beta_0 = 0.0021$.

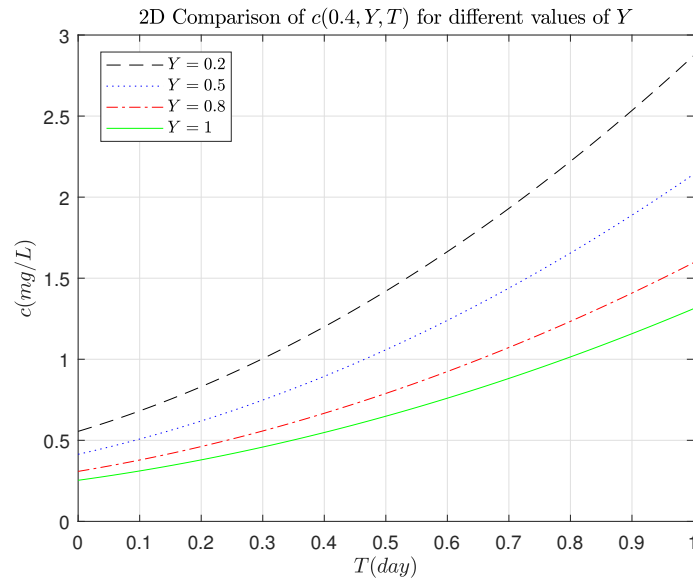


Figure 3. Two-dimensional comparison of approximate solution for different values of $Y = 0.2, 0.5, 0.8,$ and 1 for $R_0 = 1.15, u_0 = 1.05, v_0 = 0.105, \alpha_0 = 0.04, D_{x_0} = 1.25, D_{y_0} = 0.125, a = b = 0.01, \lambda = 1, \gamma_0 = 1.02,$ and $\beta_0 = 0.0021$.

The graphical depiction of concentration for various fractional order values ($\lambda = 0.22, 0.55, 0.77, 1$) at a constant period ($T = 0.3$) is shown in Figure 4. As the value of λ increases from 0 to 1, the value of c decreases.

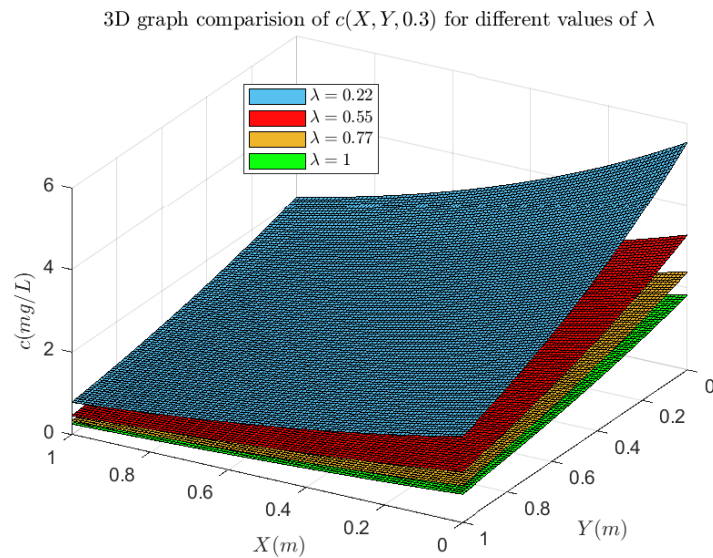


Figure 4. Behavior of approximate solution for different values of $\lambda = 0.22, 0.55, 0.77,$ and 1 for $R_0 = 1.15, u_0 = 1.05, v_0 = 0.105, \alpha_0 = 0.04, D_{x_0} = 1.25, D_{y_0} = 0.125, a = b = 0.01, T = 0.3, \gamma_0 = 1.02,$ and $\beta_0 = 0.0021$.

Figure 5 presents a visual depiction of the impact of the retardation factor on the concentration of pollutants. Tables 5 and 6 give the numerical values of pollutant concentration for different initial retardation factor $R_0 = 1.15$ and $R_0 = 2.25$, respectively, for fixed parameters $u_0 = 1.05, v_0 = 0.105, \alpha_0 = 0.04, D_{x_0} = 1.25, D_{y_0} = 0.125, a = b = 0.01, T = 0.5, \gamma_0 = 1.02$ and $\beta_0 = 0.0021$.

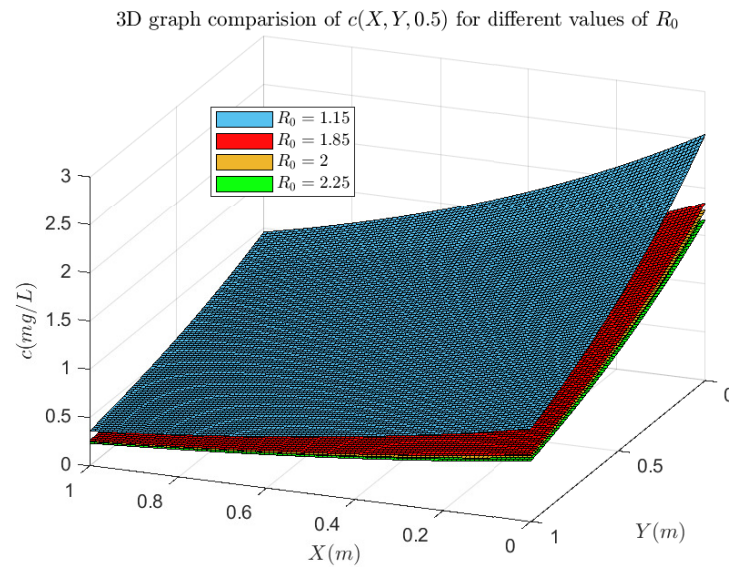


Figure 5. Comparison of the concentration profile in three dimensions for various retardation coefficients $R_0 = 1.15, 1.85, 2,$ and 2.25 for $u_0 = 1.05, v_0 = 0.105, \alpha_0 = 0.04, D_{x_0} = 1.25, D_{y_0} = 0.125, a = b = 0.01, T = 0.5, \gamma_0 = 1.02,$ and $\beta_0 = 0.0021$.

Table 5. $c(X, Y, 0.5)$ for fixed $R_0 = 1.15$.

X\Y	0.1	0.2	0.3	0.4	0.5	0.6	0.7	0.8	0.9	1
0.1	2.101758	1.905566	1.727696	1.566436	1.420236	1.287689	1.16752	1.058574	0.959801	0.870252
0.2	1.905566	1.727696	1.566436	1.420236	1.287689	1.16752	1.058574	0.959801	0.870252	0.789067
0.3	1.727696	1.566436	1.420236	1.287689	1.16752	1.058574	0.959801	0.870252	0.789067	0.715462
0.4	1.566436	1.420236	1.287689	1.16752	1.058574	0.959801	0.870252	0.789067	0.715462	0.648732
0.5	1.420236	1.287689	1.16752	1.058574	0.959801	0.870252	0.789067	0.715462	0.648732	0.588233
0.6	1.287689	1.16752	1.058574	0.959801	0.870252	0.789067	0.715462	0.648732	0.588233	0.533384
0.7	1.16752	1.058574	0.959801	0.870252	0.789067	0.715462	0.648732	0.588233	0.533384	0.483657
0.8	1.058574	0.959801	0.870252	0.789067	0.715462	0.648732	0.588233	0.533384	0.483657	0.438574
0.9	0.959801	0.870252	0.789067	0.715462	0.648732	0.588233	0.533384	0.483657	0.438574	0.397701
1	0.870252	0.789067	0.715462	0.648732	0.588233	0.533384	0.483657	0.438574	0.397701	0.360645

Table 6. $c(X, Y, 0.5)$ for fixed $R_0 = 2.25$.

X\Y	0.1	0.2	0.3	0.4	0.5	0.6	0.7	0.8	0.9	1
0.1	1.367598	1.239926	1.124177	1.019237	0.924097	0.837842	0.759642	0.688745	0.624469	0.566195
0.2	1.239926	1.124177	1.019237	0.924097	0.837842	0.759642	0.688745	0.624469	0.566195	0.513363
0.3	1.124177	1.019237	0.924097	0.837842	0.759642	0.688745	0.624469	0.566195	0.513363	0.465465
0.4	1.019237	0.924097	0.837842	0.759642	0.688745	0.624469	0.566195	0.513363	0.465465	0.42204
0.5	0.924097	0.837842	0.759642	0.688745	0.624469	0.566195	0.513363	0.465465	0.42204	0.382671
0.6	0.837842	0.759642	0.688745	0.624469	0.566195	0.513363	0.465465	0.42204	0.382671	0.346977
0.7	0.759642	0.688745	0.624469	0.566195	0.513363	0.465465	0.42204	0.382671	0.346977	0.314618
0.8	0.688745	0.624469	0.566195	0.513363	0.465465	0.42204	0.382671	0.346977	0.314618	0.28528
0.9	0.624469	0.566195	0.513363	0.465465	0.42204	0.382671	0.346977	0.314618	0.28528	0.258682
1	0.566195	0.513363	0.465465	0.42204	0.382671	0.346977	0.314618	0.28528	0.258682	0.234568

Figure 6 presents a three-dimensional graphical depiction illustrating the impact of initial velocity on the concentration of pollutants. Tables 7 and 8 present numerical values of the concentration function for various initial velocities. The values of (u_0, v_0) are $(1.05, 0.105)$ and $(2.5, 0.25)$, respectively, for the specified parameters. The values of the parameters are as follows: $R_0 = 1.15, \alpha_0 = 0.04, D_{x_0} = 1.25, D_{y_0} = 0.125, a = b = 0.01, T = 0.4, \gamma_0 = 1.02,$ and $\beta_0 = 0.0021$.

Table 7. $c(X, Y, 0.4)$ for fixed $u_0 = 1.05, v_0 = 0.105$.

X\Y	0.1	0.2	0.3	0.4	0.5	0.6	0.7	0.8	0.9	1
0.1	1.776338	1.610519	1.460186	1.323891	1.200325	1.088298	0.986733	0.894653	0.811172	0.735486
0.2	1.610519	1.460186	1.323891	1.200325	1.088298	0.986733	0.894653	0.811172	0.735486	0.666869
0.3	1.460186	1.323891	1.200325	1.088298	0.986733	0.894653	0.811172	0.735486	0.666869	0.60466
0.4	1.323891	1.200325	1.088298	0.986733	0.894653	0.811172	0.735486	0.666869	0.60466	0.54826
0.5	1.200325	1.088298	0.986733	0.894653	0.811172	0.735486	0.666869	0.60466	0.54826	0.497128
0.6	1.088298	0.986733	0.894653	0.811172	0.735486	0.666869	0.60466	0.54826	0.497128	0.45077
0.7	0.986733	0.894653	0.811172	0.735486	0.666869	0.60466	0.54826	0.497128	0.45077	0.408742
0.8	0.894653	0.811172	0.735486	0.666869	0.60466	0.54826	0.497128	0.45077	0.408742	0.370638
0.9	0.811172	0.735486	0.666869	0.60466	0.54826	0.497128	0.45077	0.408742	0.370638	0.336093
1	0.735486	0.666869	0.60466	0.54826	0.497128	0.45077	0.408742	0.370638	0.336093	0.304774

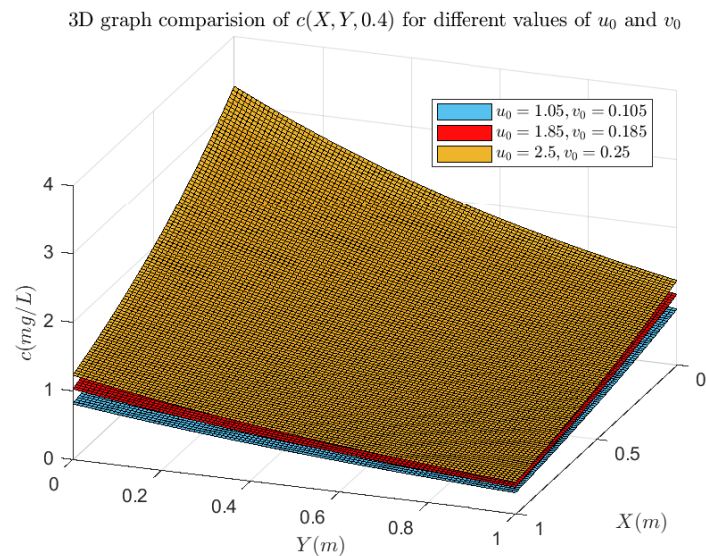


Figure 6. Comparison of the concentration profile in three dimensions for various initial velocities $(u_0 = 1.05, v_0 = 0.105), (u_0 = 1.85, v_0 = 0.185),$ and $(u_0 = 2.5, v_0 = 0.25)$ for $R_0 = 1.15, \alpha_0 = 0.04, D_{x_0} = 1.25, D_{y_0} = 0.125, a = b = 0.01, T = 0.4, \gamma_0 = 1.02,$ and $\beta_0 = 0.0021$.

Figure 7 provides a visual depiction of the impact of the dispersion coefficient on the concentration of pollutants. The numerical values of the concentration profile for different initial dispersion coefficients at various space and time intervals are shown in Tables 9 and 10. The value of initial dispersion coefficients (D_{x_0}, D_{y_0}) are $(1.25, 0.125)$ and $(2.5, 0.25)$, respectively, for the fixed parameters $R_0 = 1.15, u_0 = 1.05, v_0 = 0.105, \alpha_0 = 0.04, a = b = 0.01, T = 0.8, \gamma_0 = 1.02,$ and $\beta_0 = 0.0021$. The concentration function's value (c) drops as R_0 rises. The value of the concentration function (c) rises when (D_{x_0}, D_{y_0}) and (u_0, v_0) in the longitudinal and transverse directions are increased.

Table 8. $c(X, Y, 0.4)$ for fixed $u_0 = 2.5, v_0 = 0.25$.

X\Y	0.1	0.2	0.3	0.4	0.5	0.6	0.7	0.8	0.9	1
0.1	2.691031	2.439792	2.212015	2.005509	1.818288	1.648552	1.494666	1.355151	1.228665	1.113991
0.2	2.439792	2.212015	2.005509	1.818288	1.648552	1.494666	1.355151	1.228665	1.113991	1.010027
0.3	2.212015	2.005509	1.818288	1.648552	1.494666	1.355151	1.228665	1.113991	1.010027	0.915771
0.4	2.005509	1.818288	1.648552	1.494666	1.355151	1.228665	1.113991	1.010027	0.915771	0.830317
0.5	1.818288	1.648552	1.494666	1.355151	1.228665	1.113991	1.010027	0.915771	0.830317	0.752844
0.6	1.648552	1.494666	1.355151	1.228665	1.113991	1.010027	0.915771	0.830317	0.752844	0.682605
0.7	1.494666	1.355151	1.228665	1.113991	1.010027	0.915771	0.830317	0.752844	0.682605	0.618926
0.8	1.355151	1.228665	1.113991	1.010027	0.915771	0.830317	0.752844	0.682605	0.618926	0.561194
0.9	1.228665	1.113991	1.010027	0.915771	0.830317	0.752844	0.682605	0.618926	0.561194	0.508853
1	1.113991	1.010027	0.915771	0.830317	0.752844	0.682605	0.618926	0.561194	0.508853	0.4614

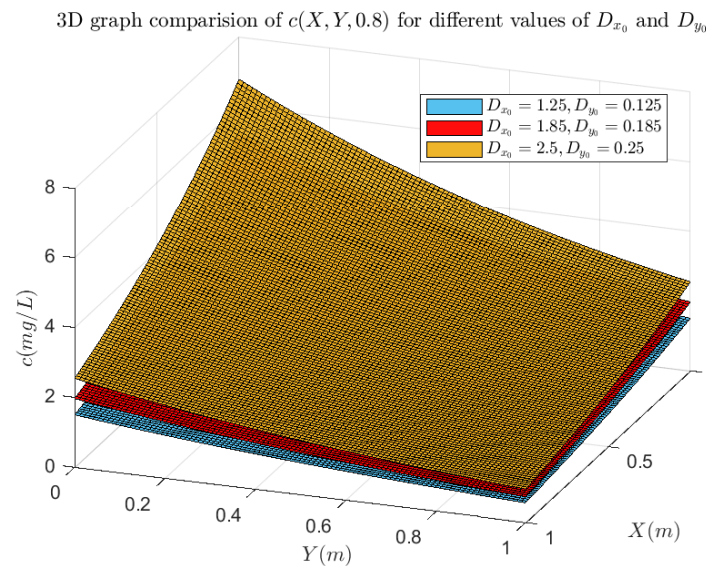


Figure 7. Comparison of the concentration profile in three dimensions for various initial dispersion coefficients ($D_{x_0} = 1.25, D_{y_0} = 0.125$), ($D_{x_0} = 1.85, D_{y_0} = 0.185$), and ($D_{x_0} = 2.5, D_{y_0} = 0.25$) for $R_0 = 1.15, u_0 = 1.05, v_0 = 0.105, \alpha_0 = 0.04, a = b = 0.01, T = 0.8, \gamma_0 = 1.02,$ and $\beta_0 = 0.0021$.

Table 9. $c(X, Y, 0.8)$ for fixed $D_{x_0} = 1.25, D_{y_0} = 0.125$.

X\Y	0.1	0.2	0.3	0.4	0.5	0.6	0.7	0.8	0.9	1
0.1	3.286394	2.979622	2.701499	2.449348	2.220745	2.013491	1.825591	1.655239	1.500795	1.360774
0.2	2.979622	2.701499	2.449348	2.220745	2.013491	1.825591	1.655239	1.500795	1.360774	1.233829
0.3	2.701499	2.449348	2.220745	2.013491	1.825591	1.655239	1.500795	1.360774	1.233829	1.11874
0.4	2.449348	2.220745	2.013491	1.825591	1.655239	1.500795	1.360774	1.233829	1.11874	1.014398
0.5	2.220745	2.013491	1.825591	1.655239	1.500795	1.360774	1.233829	1.11874	1.014398	0.9198
0.6	2.013491	1.825591	1.655239	1.500795	1.360774	1.233829	1.11874	1.014398	0.9198	0.834036
0.7	1.825591	1.655239	1.500795	1.360774	1.233829	1.11874	1.014398	0.9198	0.834036	0.756282
0.8	1.655239	1.500795	1.360774	1.233829	1.11874	1.014398	0.9198	0.834036	0.756282	0.685789
0.9	1.500795	1.360774	1.233829	1.11874	1.014398	0.9198	0.834036	0.756282	0.685789	0.621879
1	1.360774	1.233829	1.11874	1.014398	0.9198	0.834036	0.756282	0.685789	0.621879	0.563937

Table 10. $c(X, Y, 0.8)$ for fixed $D_{x_0} = 2.5$, $D_{y_0} = 0.25$.

$X \setminus Y$	0.1	0.2	0.3	0.4	0.5	0.6	0.7	0.8	0.9	1
0.1	5.577341	5.056625	4.584537	4.156536	3.768504	3.41671	3.097768	2.808611	2.546458	2.308786
0.2	5.056625	4.584537	4.156536	3.768504	3.41671	3.097768	2.808611	2.546458	2.308786	2.09331
0.3	4.584537	4.156536	3.768504	3.41671	3.097768	2.808611	2.546458	2.308786	2.09331	1.897956
0.4	4.156536	3.768504	3.41671	3.097768	2.808611	2.546458	2.308786	2.09331	1.897956	1.720846
0.5	3.768504	3.41671	3.097768	2.808611	2.546458	2.308786	2.09331	1.897956	1.720846	1.560275
0.6	3.41671	3.097768	2.808611	2.546458	2.308786	2.09331	1.897956	1.720846	1.560275	1.4147
0.7	3.097768	2.808611	2.546458	2.308786	2.09331	1.897956	1.720846	1.560275	1.4147	1.282719
0.8	2.808611	2.546458	2.308786	2.09331	1.897956	1.720846	1.560275	1.4147	1.282719	1.163064
0.9	2.546458	2.308786	2.09331	1.897956	1.720846	1.560275	1.4147	1.282719	1.163064	1.054583
1	2.308786	2.09331	1.897956	1.720846	1.560275	1.4147	1.282719	1.163064	1.054583	0.956232

5. Conclusions

The efficacy of using the fractional reduced differential transform method (FRDTM) has been shown in acquiring a two-dimensional analytical solution for the advection–dispersion problem. This approach can handle variable parameters and is used explicitly for nonreactive pollutant transport. Additionally, the FRDTM approach demonstrates a more rapid convergence of the solutions. The level of concentration has a positive correlation with the increase in time. The concentration negatively correlates with the rise in variables X and Y . When the initial retardation factor rises, there is a corresponding fall in pollutant levels. When the starting velocity and dispersion coefficient rise, there is a corresponding increase in the pollutant level. The impact of the fractional order of the Caputo derivative on the concentration of pollutants is significant. In the context of the present study, it is observed that, when the fractional order is smaller, there is an increase in the concentration of pollutants within the specified research area. The discovered solution demonstrates excellent applicability to actual instances of solute transport phenomena. An analytic solution is essential and cost-effective because it offers a more accurate physical understanding of water transport and solutes. This study will demonstrate that several methods have been provided to address this specific real-life problem to demonstrate the efficacy and efficiency of the procedure under consideration.

Author Contributions: All authors have contributed equally to the manuscript. All authors have read and agreed to the published version of the manuscript.

Funding: This research received no external funding.

Institutional Review Board Statement: Not applicable.

Informed Consent Statement: Not applicable.

Data Availability Statement: Data are contained within the article.

Conflicts of Interest: The authors declare no conflict of interest.

References

1. Liu, F.; Anh, V.V.; Turner, I.; Zhuang, P. Time fractional advection-dispersion equation. *J. Appl. Math. Comput.* **2003**, *13*, 233–245. [[CrossRef](#)]
2. Mark M.M.; Charles T. Finite difference approximations for fractional advection-dispersion flow equations. *J. Comput. Appl. Math.* **2004**, *172*, 65–77.
3. Chaves, A.S. A fractional diffusion equation to describe Lévy flights. *Phys. Lett. A* **1998**, *239*, 13–16. [[CrossRef](#)]
4. Benson, D.A.; Wheatcraft, S.W.; Meerschaert, M.M. Application of a fractional advection-dispersion equation. *Water Resour. Res.* **2000**, *36*, 1403–1412. [[CrossRef](#)]

5. Natarajan, N.; Kumar, G.S. Spatial moment analysis of colloid facilitated radionuclide transport in a coupled fracture-matrix system. *Int. J. Energy Environ.* **2011**, *2*, 491–504.
6. Ovaysi, S.; Piri, M.C. Pore-scale modeling of dispersion in disordered porous media. *J. Contam. Hydrol.* **2011**, *124*, 68–81. [[CrossRef](#)]
7. Savovic, S.; Djordjevic, A. Numerical solution for temporally and spatially dependent solute dispersion of pulse type input concentration in semi-infinite media. *Int. J. Heat Mass Transf.* **2013**, *60*, 291–295. [[CrossRef](#)]
8. Djordjevic, A.; Savovic, S.; Janicijevic, A. Explicit finite-difference solution of two-dimensional solute transport with periodic flow in homogenous porous media. *J. Hydrol. Hydromech.* **2017**, *65*, 426–432. [[CrossRef](#)]
9. Yadav, R.R.; Kumar, L.K. Two-dimensional conservative solute transport with temporal and scale-dependent dispersion: Analytical solution. *Int. J. Adv. Math.* **2018**, *2*, 90–111.
10. Saffarian, M.; Mohebbi, A. Finite difference/spectral element method for one and two-dimensional Riesz space fractional advection–dispersion equations. *Math. Comput. Simul.* **2022**, *193*, 348–370. [[CrossRef](#)]
11. Zhang, H.; Liu, F.; Jiang, X.; Turner, I. Spectral method for the two-dimensional time distributed-order diffusion-wave equation on a semi-infinite domain. *J. Comput. Appl. Math.* **2022**, *399*, 113712. [[CrossRef](#)]
12. Ahmed, N.; Shah, N.A.; Vieru, D. Two-dimensional advection–diffusion process with memory and concentrated source. *Symmetry* **2019**, *11*, 879. [[CrossRef](#)]
13. Yadav, R.R.; Kumar, L.K. Solute transport for pulse type input point source along temporally and spatially dependent flow. *Pollution* **2019**, *5*, 53–70.
14. Hadhouda, M.K.; Hassan, Z.S. Mathematical model for unsteady remediation of river pollution by aeration. *Inf. Sci. Lett.* **2022**, *11*, 323–329.
15. Patel, H.; Patel, T.; Pandit, D. An efficient technique for solving fractional-order diffusion equations arising in oil pollution. *J. Ocean. Eng. Sci.* **2023**, *8*, 217–225. [[CrossRef](#)]
16. Alshammari, S.; Abuasad, S. Exact solutions of the 3D fractional helmholtz equation by fractional differential transform method. *J. Funct. Spaces* **2022**, *2022*, 7374751. [[CrossRef](#)]
17. Patel, T.; Patel, H. An analytical approach to solve the fractional-order (2+1)-dimensional Wu–Zhang equation. *Math. Methods Appl. Sci.* **2023**, *46*, 479–489. [[CrossRef](#)]
18. Osman, M.; Xia, Y.; Omer, O.A.; Hamoud, A. On the fuzzy solution of linear-nonlinear partial differential equations. *Mathematics* **2022**, *10*, 2295. [[CrossRef](#)]
19. Al-Amr, M.O. New applications of reduced differential transform method. *Alex. Eng. J.* **2014**, *53*, 243–247. [[CrossRef](#)]
20. Moosavi Noori, S.R.; Taghizadeh, N. Study of convergence of reduced differential transform method for different classes of differential equations. *Int. J. Differ. Equations* **2021**, *2021*, 6696414. [[CrossRef](#)]
21. Noori, S.R.M.; Taghizadeh, N. Study of convergence of reduced differential transform method for different classes of nonlinear differential equations. *Authorea Prepr.* **2020**. [[CrossRef](#)]
22. Varsoliwala, A.C.; Singh, T.R. Mathematical modeling of atmospheric internal waves phenomenon and its solution by Elzaki Adomian decomposition method. *J. Ocean. Eng. Sci.* **2022**, *7*, 203–212. [[CrossRef](#)]
23. Tandel, P.; Patel, H.; Patel, T. Tsunami wave propagation model: A fractional approach. *J. Ocean. Eng. Sci.* **2022**, *7*, 509–520. [[CrossRef](#)]
24. Singh, B.K.; Kumar, P. FRDTM for numerical simulation of multi-dimensional, time-fractional model of Navier–Stokes equation. *Ain Shams Eng. J.* **2018**, *9*, 827–834. [[CrossRef](#)]
25. Abuasad, S.; Moaddy, K.; Hashim, I. Analytical treatment of two-dimensional fractional Helmholtz equations. *J. King Saud-Univ.-Sci.* **2019**, *31*, 659–666. [[CrossRef](#)]
26. Al-rabtah, A.; Abuasad, S. Effective Modified Fractional Reduced Differential Transform Method for Solving Multi-Term Time-Fractional Wave-Diffusion Equations. *Symmetry* **2023**, *15*, 1721. [[CrossRef](#)]

Disclaimer/Publisher’s Note: The statements, opinions and data contained in all publications are solely those of the individual author(s) and contributor(s) and not of MDPI and/or the editor(s). MDPI and/or the editor(s) disclaim responsibility for any injury to people or property resulting from any ideas, methods, instructions or products referred to in the content.